8th U. S. National Combustion Meeting
Organized by the Western States Section of the Combustion Institute
and hosted by the University of Utah
May 19-22, 2013

Sensitivity Analysis of Particle Formation in a Spark-Ignition Engine during Premixed Operation

Mitchell Hageman[1] *David Rothamer*[2]

[1]*Engine Research Center, University of Wisconsin, Madison, 1500 Engineering Drive, Madison, WI*
[2] *Engine Research Center, University of Wisconsin, Madison, 1500 Engineering Drive, Madison, WI*

An experimental sensitivity analysis was performed on a spark-ignition engine to determine the response of a premixed flame to changes in fundamental parameters with regard to particle formation. The parameters varied were intake pressure, intake temperature, and equivalence ratio. A certification gasoline was used for all experiments. Premixing was accomplished by injecting the fuel at high pressure into the intake air stream well upstream of the intake port, providing enough residence time to ensure complete mixing of the air/fuel mixture. A three factor, two level (2^3) factorial design with a center point was used for the initial set of tests, resulting in nine test points with a systematic set of combinations of the three variables. Particulate size distributions were measured using a scanning mobility particle sizer (SMPS). The study showed significant dependence of particulate formation on all three variables studied. A second set of tests were performed to investigate the influence of equivalence ratio on particulate formation under premixed conditions. The data showed a significant number of small particles exist for stoichiometric and lean operating conditions with diameters less than 50 nm. For equivalence ratios less than 1.2 the measured particle size distribution is relatively invariant with respect to equivalence ratio indicating that bulk gas formation is likely not the source of the particulate under these conditions, due to the high peak temperatures and premixed air-fuel distribution. Future work will focus on determining the source of these particles as it potentially serves as a mechanism for particulate generation in all spark-ignition engines.

1. Introduction

The European Union instituted the particulate measurement program (PMP) to validate new particle measurement methods that can offer data on particle number emissions as well as mass-based emissions (UN 2010). The PMP method is used to measure particulate emissions over the new European driving cycle (NEDC). The Euro 6 regulation specifies a particulate number (PN) limit for spark-ignition direct-injection (SIDI) vehicles of 6×10^{12} particles/km for vehicles produced after September 2014. After 3 years the Euro 6 regulations drop to a limit of 6×10^{11} particles/km (He, Ratcliff et al. 2012). In the United States, the current Tier 2 bin 5 particulate limit is 10 mg/mi for the federal test procedure-75 (FTP -75) test cycle (Chan, Meloche et al. 2012). However, the California Air Resources Board (CARB) has implemented tighter standards for vehicles to meet the LEV III regulation. A phased reduction is implemented in the LEV III regulations with a 3 mg/mi PM standard phasing in between 2017 and 2021 and a 1 mg/mi standard phasing in from 2025 to 2028 on the FTP-75 drive cycle. It is likely that many current SIDI engine designs may have difficulty meeting these limits (Piock, Hoffmann et al. 2011).

Significant research effort has been given to investigating the operating conditions that affect particulate number emissions from SIDI engines. The literature regarding effects of mixing and injection strategies, combustion phasing, load, engine speed, ethanol mixtures, and transient effects is extensive. For a given operating condition in a SIDI engine, there are many potential sources of particulates. Incomplete mixing and wall wetting are often cited as the primary sources of particulates (Zhao, Lai et al. 1999; Piock, Hoffmann et al. 2011; He, Ratcliff et al. 2012). However, the relative magnitude of these two factors compared to other potential sources of particulates has not been quantified. In order to meet future emissions regulations without the use of a particulate filter will require SIDI engines to have

particulate emissions nearly as low as their port fuel-injection counterparts. For this to be achieved requires an understanding of all sources of particulate even those not related to the fuel injection and mixing process. Therefore, the baseline sources of particulate formation present under nearly homogeneous conditions are of importance. Even if particulate filters are used to meet emissions regulations, an understanding of the particulate size distribution is necessary for optimization of filter design, and an understanding of how different particulate formation mechanisms influence the particle size distribution and particulate composition is needed.

A systematic determination of the individual contributions of different parameters to the total particulate count is difficult under direct-injected (DI) operation because the mixing and impingement characteristics change with each of the other parameters making it impossible to isolate any single parameter. Relevant examples of this for the current study include those associated with intake temperature, intake pressure, and equivalence ratio. Greater in-cylinder pressure directly affects the reaction kinetics of combustion (Bonig, Felderman et al. 1990; Mauss and Bockhorn 1995; Liu, Thomson et al. 2006; Joo and Gulder 2009), but it also affects spray penetration and charge motion altering mixture preparation (Zhao, Lai et al. 1999). Intake air temperature influences the in-cylinder temperature history impacting particle inception (Haynes and Wagner 1981; Kayes and Hochgreb 1999), but also impacts spray vaporization (Zhao, Lai et al. 1999; Piock, Hoffmann et al. 2011). Finally, the fuel flow rate directly controls the ratio of fuel-to-air in-cylinder and is a function of injector duration and pressure, both of which directly affect mixture preparation (Zhao, Lai et al. 1999; Piock, Hoffmann et al. 2011; Choi, Kim et al. 2012). Each of these mixing side-effects present for direct-injection operation can be eliminated by fully premixing the fuel and air well upstream of the combustion chamber; this potentially allows the effects of temperature, pressure, and equivalence ratio to be systematically isolated.

The goal of this study was to eliminate the confounding effects of incomplete mixing and to begin to isolate the contributions of temperature, pressure, and equivalence ratio on particle formation under homogeneous conditions. The results provide insight into the baseline particulate level that is likely to be present for nearly homogeneous in-cylinder mixtures. Additionally, the 2^3 factorial design highlights the relative contributions of each of these three parameters, and the interdependencies between the parameters in a premixed flame engine environment.

2. Methods

Experimental Setup

Engine

The engine geometric specifications are given in Table 1. A spark-ignition direct-injection (SIDI) cylinder head with pentroof geometry was utilized. The compression ratio with the flat-top piston used is 11.97. For this study, the DI fuel injector remained installed, but was unused. Another injector was mounted in a premixing chamber upstream of the intake surge tank. This allows the fuel and air to mix thoroughly in the heated intake stream before entering the cylinder. The spark plug is centered at the top of the combustion chamber between the intake and exhaust valves.

Table 1: Engine geometry specifications

Dimension	Unit	Value
Compression Ratio	[-]	11.97
Bore	[mm]	85.96
Stroke	[mm]	94.6
Connecting Rod Length	[mm]	152.4
Clearance Volume	[cm^3]	50.0
Intake Valve Lift	[mm]	9.9
Exhaust Valve Lift	[mm]	9.9
Intake Valve Open	[$^\circ$bTDC]	10
Intake Valve Close	[$^\circ$aTDC]	220
Exhaust Valve Open	[$^\circ$aTDC]	150
Exhaust Valve Close	[$^\circ$aTDC]	5
Displacement	[cm^3]	549.0

The fuel used in this study was an EPA Tier II EEE certification fuel (Haltermann Products). Properties for the fuel are shown in Table 2. In-cylinder pressure was measured using a piezoelectric pressure transducer (Kistler model# 6125). The measured pressure was used to determine indicated mean effective pressure (IMEP) and location of 50% cumulative heat release (CA50). A MATLAB post-processing program utilized the pressure data to calculate the cumulative heat release, heat release rate, and cylinder temperature history using an ideal gas approximation and a method similar to that of Gatowski et al. (Gatowski, Balles et al. 1984).

Table 2: Properties of Tier II EEE research fuel

Property	Unit	Value
Density	[kg/L]	0.742
Reid Vapor Pressure	[kPa]	62
Lower heating Value	[MJ/kg]	42.786
Hydrogen/Carbon Ratio	[-]	1.873
Research Octane Number	[-]	97

Particulate Sampling System

Particle size distributions (PSDs) were measured over the mobility diameter range from 7 nm to 300 nm using a scanning mobility particle sizer (SMPS). The SMPS system is composed of a long differential mobility analyzer (DMA, TSI, model 3081) controlled by an electrostatic classifier (EC, TSI, model 3080) followed by a condensation particle counter (TSI, model 3010). Particulate data were processed using the Aerosol Instrument Manager (AIM) software (TSI) supplied with the SMPS. All data presented here utilize both the diffusion correction option and the multiple charge correction options in the AIM software.

The SMPS receives an engine-out exhaust sample that has been diluted using a micro-dilution system (Dekati FPS-4000). The dilution system takes a raw sample from the exhaust stream via a probe located downstream of the exhaust surge tank. The exhaust at the sample point generally reaches a steady state temperature of about 275°C; the probe is heated to approximately 250°C to maintain a nearly isothermal sampling point. The sample then undergoes a two-stage dilution process. The first stage utilizes heated filtered air intended to provide a near isothermal dilution and avoid any modification of the particles via adsorption or absorption of hydrocarbons. The second stage provides cold dilution by sending the sample through an ejector diluter using filtered, room-temperature air so that the sample is cooled sufficiently before entering the particle counting system. The output of the micro-diluter is split between an insulated line that leads to the inlet of the particulate sampling system, a CO_2 analyzer, and an excess flow tube that is plumbed into the building exhaust system. The CO_2 sample from the dilution system is compared to the CO_2 concentration in the raw exhaust sample to determine the dilution ratio. A flow diagram of the entire exhaust sampling system is shown in Figure 1. Studies have been performed with a range of dilution ratios to ensure that the measurements are not sensitive to the dilution ratio for the range of conditions tested in the current study.

Emissions Measurements

A Horiba emissions bench was used to sample engine-out, undiluted gaseous emissions. The bench includes a flame ionization detector (FID) for total hydrocarbons (Horiba, FIAA-23A), a non-dispersive infrared analyzer (Horiba, AIA-23) to measure both CO and CO_2 concentrations, a chemiluminescent analyzer to measure NO_X (Horiba, CLA-22A), and a magnetopneumatic analyzer for O_2 measurements (Horiba, MPA-21A). These emissions measurements were used to determine oxygen- and carbon-based air-fuel ratios, and the total dilution ratio achieved by the dilution system.

Experimental Matrix

The 2^3 factorial design of the sensitivity study was used to simultaneously test the sensitivity of the PSD and thermodynamic conditions to wide changes in the equivalence ratio (Φ), intake temperature, and intake manifold pressure (IMAP). Two intake temperatures, two intake manifold pressures, and two equivalence ratios were chosen along with a single center point consisting of mid-point value for all three parameters, resulting in nine unique operating points. These points are summarized in Table 3.

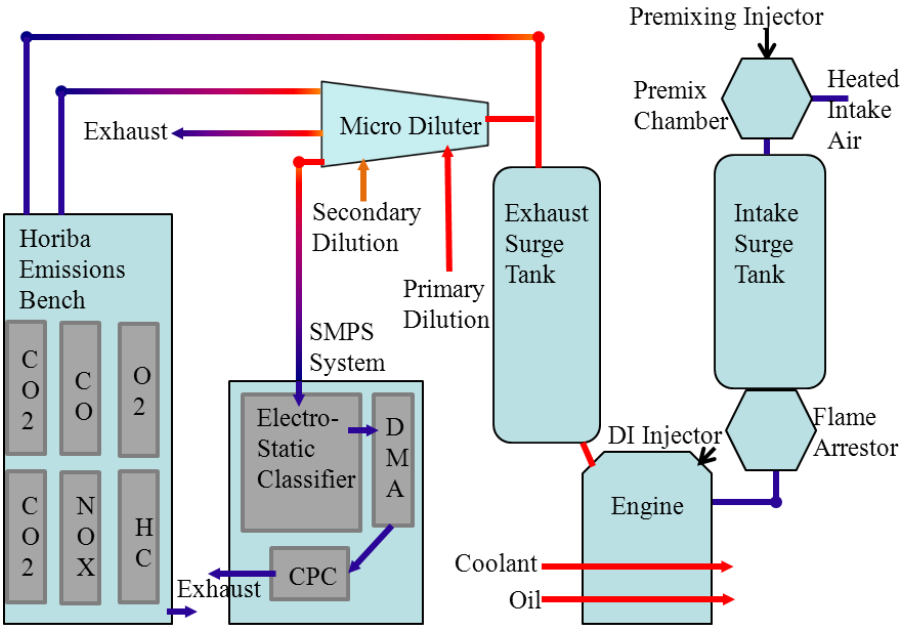

Figure 1: Flow Diagram of intake, engine, and exhaust systems

Table 3: Control parameters for 2^3 factorial sensitivity study with center point

Φ	0.98	0.8	0.8	0.8	0.8	1.2	1.2	1.2	1.2
C/O	0.33	0.26	0.26	0.26	0.26	0.41	0.41	0.41	0.41
T_{in} [°C]	80	40	40	120	120	40	40	120	120
IMAP [kPa]	52.5	39	65.5	39	65.5	39	65.5	39	65.5
IMEP [kPa]	445.1	269.1	552.9	235	468.2	344.1	677.5	295	569
COV of IMEP [%]	2.7	6.0	3.3	4.9	3.0	2.5	1.8	2.5	1.9
CA50 [CAD]	17.9	17.9	17.6	17.7	18.2	17.8	17.7	17.9	17.8

The intake temperatures were controlled using intake air heaters and a well-insulated intake runner. Heating of the intake charge increases the IMAP for a fixed air mass flow rate. However, it was desired to keep IMAP constant as intake temperature was varied, which required a reduction in the air mass flow rate at the higher intake temperature. Therefore, for the same IMAP and a higher intake temperature, maintaining Φ required a slightly lower fuel mass flow rate. The higher manifold pressures are representative of higher engine load, and were achieved by increasing intake fuel and air flow rates. When varying Φ, it was possible to maintain intake temperature and IMAP using nearly the same air flow rate, so the equivalence ratio was controlled primarily by changing the fuel mass flow rate.

All conditions were run at an engine speed of 2100 rpm and a CA50 of 18° after top-dead-center (aTDC) ± 1 crank angle degree (CAD). The pressure traces show that this combustion phasing was not necessarily optimal, as evidenced by the slight bimodal shape of some of the pressure traces. This timing was necessary to prevent engine knock in the rich, high temperature, high pressure cases, and was kept constant across the sensitivity study in order to achieve better isolation of the parameters of interest.

3. Results and Discussion

The parameters of interest in this study are the in-cylinder temperature history, the in-cylinder pressure history, and Φ. Because the charge is premixed well upstream of the intake port, it is a good approximation that Φ is uniform until ignition and global and local equivalence ratios are equal and easily controlled using fuel flow. The in-cylinder temperature and pressure are slightly more difficult to control. Intake temperature and intake pressure were used to alter the in-cylinder histories because these are easily measured and can be directly controlled. However, both in-cylinder temperature and in-cylinder pressure depend on a combination of intake temperature, intake pressure, and Φ. Therefore,

the in-cylinder temperature and pressure history are more difficult to directly control, and in the current lab setup, they can only be determined during post-processing.

Sensitivity Study Results

To first order, changes in intake temperature and intake pressure should independently vary the in-cylinder temperature and in-cylinder pressure. As seen in Figure 2, Figure 3, and Table 4 this is an approximation and as the intake temperature is increased at a fixed pressure and Φ, the in-cylinder pressure decreases by approximately 10% due to increased heat transfer and changes in the specific heat ratio. When increasing intake pressure at constant intake temperature and Φ, the in-cylinder temperature increases slightly and the location of peak temperature is advanced. The change in equivalence ratio from 0.8 to 1.2 at a fixed intake temperature and pressure increases peak temperature by approximately 500 K and increases pressure by approximately 20% on average. These impacts are due to the influence of Φ on the adiabatic flame temperature, which peaks slightly rich of stoichiometric, and the influence of Φ on the flame speed (also peaks slightly rich of stoichiometric) and its subsequent impact on the overall combustion duration. The equivalence ratio also impacts temperature through the change in specific heat ratio for the reactants and products.

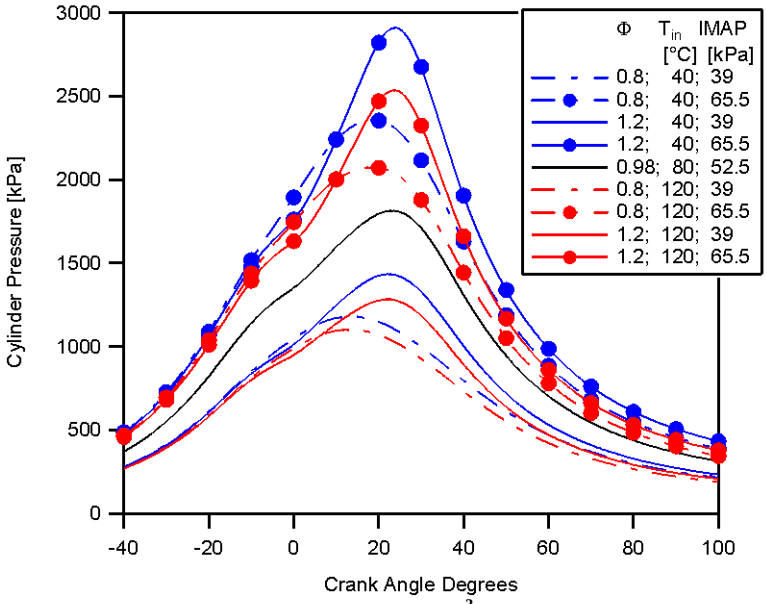

Figure 2: Cylinder pressure traces from 2^3 factorial sensitivity study

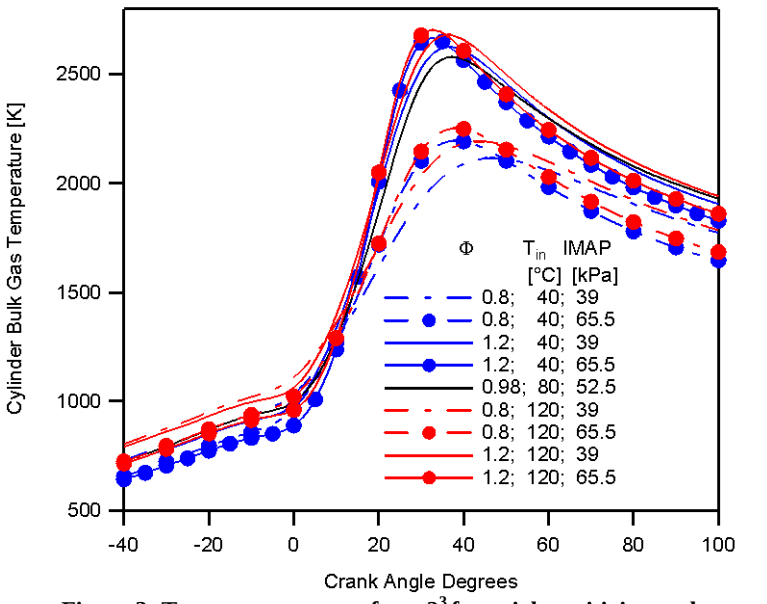

Figure 3: Temperature traces from 2^3 factorial sensitivity study.

Table 4: Experimental temperature and pressure measurements for 2^3 factorial sensitivity study

Φ	T_{in}	IMAP	Peak Cylinder Pressure	Peak Cylinder Temperature	EVO – 5 CAD Temperature	Exhaust Port Temperature
-	°C	kPa	MPa	K	K	K
0.8	40	39	1.18	2115	1594	843
		65.5	2.36	2195	1470	858
	120	39	1.1	2193	1606	828
		65.5	2.07	2252	1506	864
0.98	80	52.5	1.81	2579	1733	920
1.2	40	39	1.43	2625	1702	854
		65.5	2.91	2665	1632	881
	120	39	1.28	2680	1737	840
		65.5	2.54	2703	1666	882

Table 4 lists the exhaust port temperature and exhaust-valve-open (EVO) temperature for each case. The temperature at exhaust valve opening was reported as the value 5 CAD before EVO (EVO – 5 CAD) to ensure that the temperature reported was for the closed system before the valve opens. The exhaust port temperature is measured using a shielded k-type thermocouple inserted in the exhaust stream immediately downstream of the exhaust port. The temperature in the exhaust port is highly affected by heat transfer. Higher load conditions have higher exhaust flowrates and tend to maintain a hotter exhaust temperature even if the in-cylinder temperature was not necessarily higher.

Several studies under DI operation predated and motivated this study (Farron 2010; Matthias, Farron et al. 2011; Sakai, Hageman et al. 2013). The total particulates produced under premixed operation were generally lower than with similar studies under DI operation. In particular, the mean particle size for the homogeneous cases is smaller than for similar DI engine conditions. This agrees with the theory that incomplete mixing is a primary contributor to particulate formation (Maricq, Podsiadlik et al. 1999; Zhao, Lai et al. 1999; Price, Twiney et al. 2007; Piock, Hoffmann et al. 2011; Choi, Kim et al. 2012; Myung and Park 2012). However, a significant number of particulates remained in all cases, and several interesting trends were noted. One particular trend of interest is that in the transition from DI to premixed operation, the majority of the particle reduction occurred for particles greater than approximately 30 nm (the cutoff diameter for the PMP protocol is 23 nm). In a few of the premixed cases, the concentrations for $D_m < 20$ nm particles were actually higher than in similar DI cases.

The influence of input parameters on the particulate size distribution is shown in Figure 4. The main effects and interactions calculated from the four replicated changes in each variable are given in Table 5. From Table 5 it is apparent that the main effects for varying intake temperature, IMAP, or Φ, and the interaction effects, involving simultaneous changes in more than one variable, are all of similar magnitude. Indicating that the direct and interaction effects are all of approximately equal importance and any one of them should not be viewed alone. With that being said, with all other factors held constant: cases with low equivalence ratio resulted in fewer particulates than their high equivalence ratio counterparts, cases with higher inlet pressure resulted in fewer particulates for mobility diameters greater than 23 nm than cases with lower inlet pressure, and cases with higher inlet temperature resulted in an increase in small particles ($D_m < 23$ nm). On average, increasing variables from their low to higher values increased total particles for all variables and interactions. However, the small particles ($D_m < 23$ nm) and larger agglomerates showed differing behaviors, with the small particles always increasing with increased parameter values, whereas the agglomerate particles only increased for increased equivalence ratio and for simultaneously increasing equivalence ratio and temperature. The effects listed in Table 5 highlight the complex interaction of variables and reflect the fact that changing any one of the three intake variables ($T_{in,}$ IMAP, or Φ) actually changes both the temperature and pressure history in-cylinder.

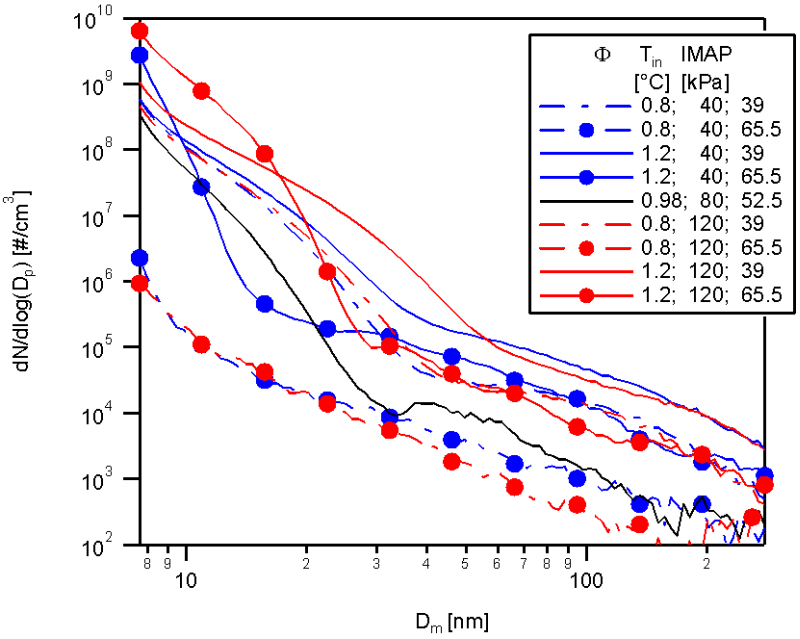

Figure 4: Particulate size distributions for 2^3 factorial study

Table 5: Main effects and interactions calculated for 2^3 factorial design variables

	Particle Number [#/cm^3]		
	Total	< 23 nm	> 23 nm
Main effects			
Phi	1.47E+08	1.47E+08	3.20E+05
IMAP	7.98E+07	8.02E+07	-3.59E+05
T_{in}	9.32E+07	9.30E+07	2.15E+05
Two-factor interactions			
Phi × T_{in}	9.53E+07	9.51E+07	1.95E+05
Phi × IMAP	1.18E+08	1.18E+08	-2.76E+05
T_{in} × IMAP	7.54E+07	7.56E+07	-2.21E+05
Three-Factor interactions			
Phi×T_in×IMAP	7.34E+07	7.36E+07	-1.99E+05

Equivalence Ratio Effect

The fact that decreasing equivalence ratio was shown to suppress soot formation was expected and is well known, but the reasoning for why this is the case in the engine is somewhat more involved due the simultaneous changes in pressure and temperature when changing Φ. Temperatures and pressures are higher for the high Φ cases indicating the possibility of both faster inception and faster oxidation. Oxidation during the particle inception stage competes with aromatics growth to remove carbon and hydrogen molecules from the sooting pathway (Frenklach 2002). The much higher oxygen concentrations for the low equivalence ratio case in the post flame regions in-cylinder, where temperatures are high enough for soot formation, results in higher oxidation rates. Therefore, lower C/O (higher oxygen availability, lower Φ) is well-known to decrease particulate number and mass (Farron, Matthias et al. ; Kayes and Hochgreb 1999; Kayes and Hochgreb 1999; Melton, Inal et al. 2000; Hsieh, Chen et al. 2002; Price, Twiney et al. 2007; Lee, Patel et al. 2009; Chen, Braisher et al. 2010; Farron 2010; Matthias, Farron et al. 2011).

However, the dependence on C/O is not as simple as the sensitivity study may suggest. A separate set of experiments was conducted under premixed operation where only the equivalence ratio was varied. For this equivalence ratio sweep, the IMEP and CA50 were held constant at 334 kPa and 8 CAD aTDC using slight variations in spark timing and charge mass, but the peak cylinder temperatures and pressures were allowed to vary. The equivalence ratio was swept from 0.8 up to 1.5, which represents a C/O sweep from C/O = 0.26 up to C/O = 0.51. Table 6 lists the equivalence ratios studied in this data set along with their corresponding C/O ratios. The in-cylinder temperature history remained relatively constant for the equivalence ratio range from 0.98 to 1.5 and the in-cylinder pressure history was also nearly constant due to the matched IMEPs.

Table 6: EEE Equivalence ratio test points and corresponding C/O ratios

ϕ	0.8	0.97	1.1	1.2	1.3	1.35	1.4	1.5
C/O	0.26	0.33	0.37	0.41	0.44	0.46	0.48	0.51
IMEP [kPa]	332.8	333.4	332.9	334.9	333.4	335.1	332.2	333.1
COV of IMEP [%]	1.3	0.8	0.8	0.7	0.9	0.8	1.0	1.1
CA50 [CAD]	8.2	7.7	8.3	7.6	8.1	7.7	8.2	8.0

The PSDs from this sweep are shown in Figure 5. There is a broad range of equivalence ratios in which increasing or decreasing the equivalence ratio does not change the PSD with any monotonic trend for Φ = 0.8 to 1.3. The PSD remains nearly the same until about Φ =1.3, at which point, the particulate number begins to increase consistently with increasing equivalence ratio. In the sensitivity study, there was a clear difference between Φ = 0.8 and Φ = 1.2 with the concentrations of particles increasing with increasing Φ. In the equivalence ratio sweep the particulate concentrations are actually higher for small particle sizes for the Φ = 0.8 condition. The difference between the results of the sensitivity study and the Φ sweep is most likely due to the differences in conditions for the two studies. For the sensitivity study the IMEP was allowed to vary, so there are significant differences in peak pressure between Φ = 0.8 and Φ = 1.2. For the Φ sweep, IMEP is constant, and the in-cylinder pressure is matched as shown in Figure 6, however, the temperature is still substantially lower for the lean condition. It is also important to note the combustion phasing as indicated by CA50 was significantly different for the sensitivity study and equivalence ratio sweep. Because of the large number of differences in the two studies it is difficult to pinpoint the reason for the differing behavior.

The key take away from the equivalence ratio sweep is that there does appear to be a threshold type behavior for significant formation of larger agglomerates which appears to occur around a critical C/O ratio of 1.35. The in-cylinder pressure and temperature histories are reasonably matched in the equivalence ratio range from 1.2 to 1.5 giving some confidence in the threshold behavior displayed. The relative insensitivity to equivalence ratio for equivalence ratios from 1 to 1.3 is also interesting and merits further study. It brings into question the origin of the particulates in this equivalence ratio range.

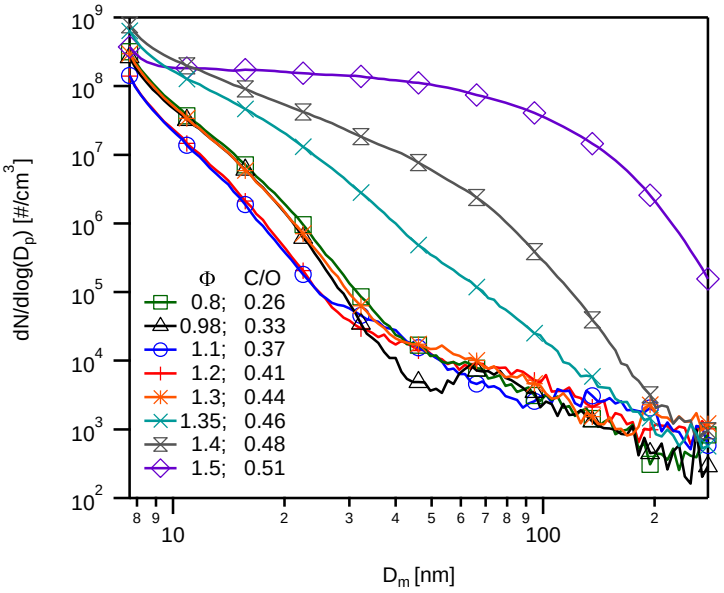

Figure 5: PSDs from premixed equivalence ratio sweep

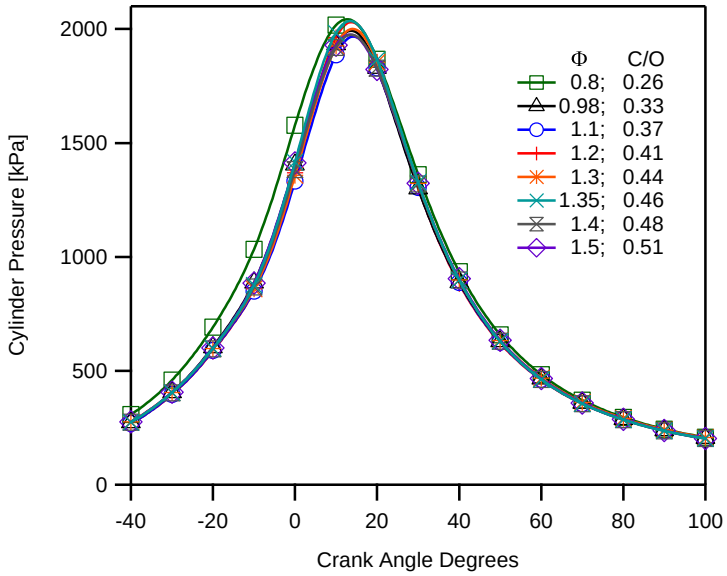

Figure 6: Cylinder pressure traces from premixed equivalence ratio sweep

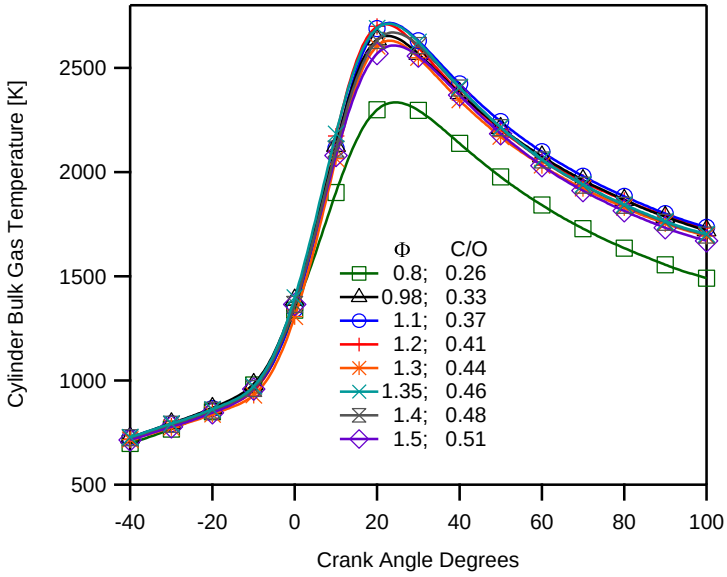

Figure 7: In-cylinder bulk gas temperature from premixed equivalence ratio sweep

Intake Pressure and Temperatures Effects

To begin the discussion, it is worth noting that general trends exist between temperature and pressure and particulate formation in premixed flames, and these trends have been well-documented in steady-state laboratory flames. The Nagle and Strickland-Constable model for oxidation is dependent on a set of Arrhenius reaction rate relationships and includes dependence on both O_2 concentration and temperature (Haynes and Wagner 1981). The critical C/O where particle inception begins for a given fuel is temperature and pressure dependent. Particle inception is known to follow an Arrhenius rate that is proportional to the presence of precursors and is exponentially dependent on temperature (Kayes and Hochgreb 1999). After soot inception, the Nagle and Strickland-Constable model shows that the surface oxidation rate initially increases exponentially with temperature until the reactive surface sites are depleted, at which point the temperature dependence decreases (Haynes and Wagner 1981) and the formation on unreactive sites becomes dominant. Once the surface of the particle is completely covered with unreactive sites, the oxidation rate once again increases with temperature. Pyrolysis reduction at high temperatures is also due in part to reverse reactions with high activation energies that cannot occur at lower temperatures (Mauss and Bockhorn 1995).

Bonig and Feldermann (Bonig, Felderman et al. 1990) showed, for a C_2H_4-air flame at a pressure of 10 bar, two types of dependence on temperature: first, they showed that for a given C/O ratio there is a low-end temperature below which particles will not form in the time allowed, and a high end temperature above which no measureable soot existed; second, between these two temperatures a bell-shaped dependence of soot volume fraction on temperature was shown. This study is relevant here because it suggests that there may be portions of the combustion cycle that can be ignored with respect to the interpretation of particulate formation because the temperature and pressure combination is outside of the range where particulates are likely to form.

Studies on premixed laboratory flames at low pressures (relative to engine pressure) have shown that the proportionality of the soot volume fraction is approximately P^2 in the range 100-300 kPa, $\sim P^{1.3}$ in the range 300-500 kPa, and drops to $\sim P^1$ at 1,000 kPa (Bonig, Felderman et al. 1990; Mauss and Bockhorn 1995). The dependence on pressure is linked to the pressure dependence of reaction rates of key species. At pressures below 1,000 kPa in a flat premixed C_2H_4 flame experiment (Bonig, Felderman et al. 1990), the maximum C_2H_2 concentration in the fast reaction zone increased with pressure, making more C_2H_2 available for formation of aromatics, suggesting that pressure is a greater factor in particle inception than in particle growth. In a separate study (Mauss and Bockhorn 1995), it was suggested that near 1000 kPa, an increase in the partial pressure of H_2 would reduce the number of radical surface sites, which may explain the decreasing dependence as pressure increases. Studies have been conducted on C_2H_4 flames all the way up to 70 bar, and particulate formation was shown to continue to rise with pressure throughout this range (Bonig, Felderman et al. 1990).

The literature on the effects of temperature and pressure on particulate formation in steady-state laboratory flames provides a good starting point for interpreting the results of this study. However, the dependence on these two parameters will be much more dynamic in the variable volume combustion chamber of an internal combustion engine, where both temperature and pressure change with time, and there is a limited chemical timescale. To make the relationships more clear, the changes in pressure and temperature for selected cases are discussed below along with the corresponding PSDs.

Intake Pressure

The plots in Figure 8 and Figure 9 demonstrate the influence of intake pressure on in-cylinder pressure, in-cylinder temperature, and the particulate size distribution. The thermodynamic results of changing the intake pressure for both the rich and lean cases are shown in Figure 8 for an intake temperature of 40°C (results for 120°C case are similar), and the PSDs are shown in Figure 9. The temperature traces for the two sets of conditions highlight the fact that there is also a notable difference in the temperature histories of the compared cases.

The cases with high intake pressure start combustion at a higher pressure, and remain at a higher pressure throughout the combustion duration. The pressure during combustion varies between 0.75 and 3.0 MPa, and the PSDs shows that the higher pressure cases result in lower particulate concentrations for particle sizes >10 nm for both lean and rich combustion. This does not tell us exactly when in the cycle or for which pressures the majority of particles are formed, but it is very clear that for the higher intake pressure conditions particle number is lower for mobility diameters greater than 10 nm for both the lean and rich equivalence ratios tested.

The particulate distributions from this study show a decrease in particulates with mobility diameter > 10 nm with increased pressure, which is counter to the results shown for laboratory flames. As mentioned earlier soot formation has been shown to be most significant in the temperature range from 1500 K to 1900 K. Looking at the in-cylinder temperature histories in Figure 3 and Figure 8 it is seen that this temperature range is not reached until approximately 60 to 80 CAD. The higher intake pressure conditions actually have lower temperatures at this time and the in-cylinder temperatures remain lower during the remainder of the expansion and exhaust strokes. It is hypothesized that the reason for the higher particulate emissions for the lower intake pressure conditions may be due in part to the higher temperatures during the second half of the expansion stroke. This appears to be supported by the larger difference in particulates between the low and high intake pressure cases for $\Phi = 0.8$ relative that those for $\Phi = 1.2$. The temperature difference between the low and high intake pressure conditions is larger for the $\Phi = 0.8$ cases and the difference in total particulates is also larger.

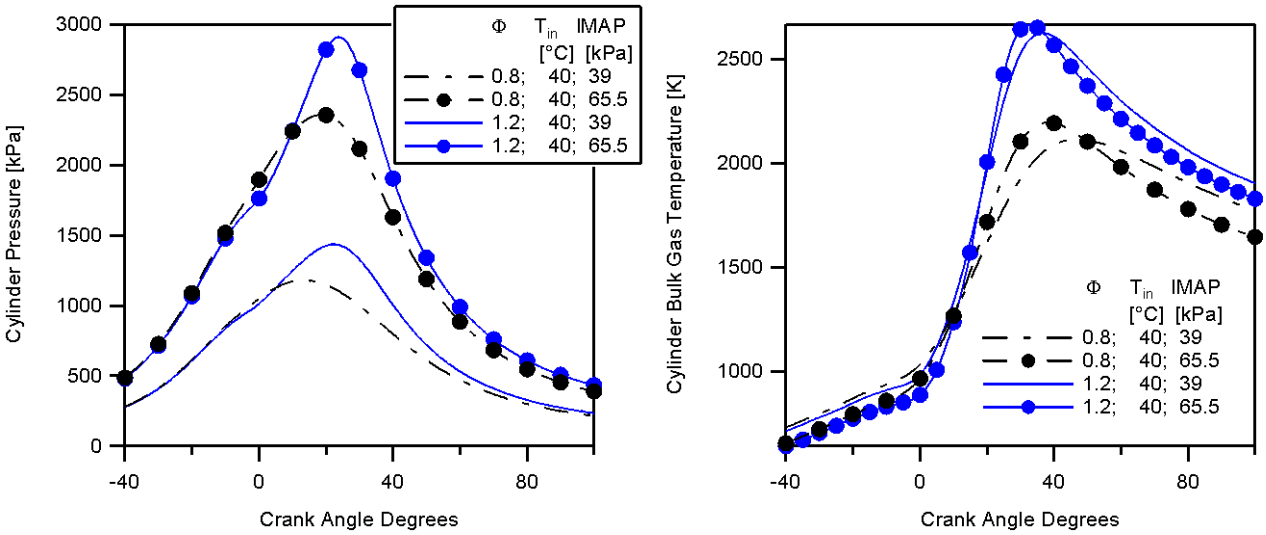

Figure 8: Temperature and pressure traces comparing high and low pressure cases

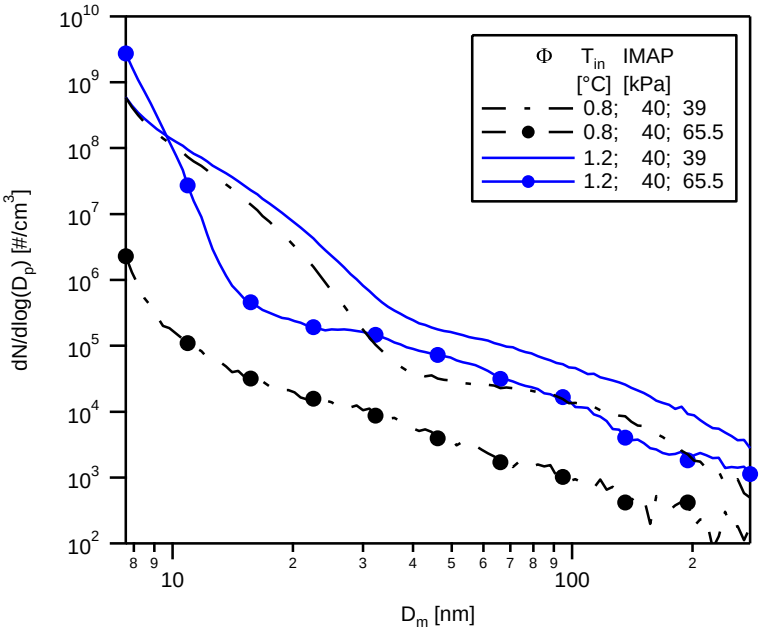

Figure 9: PSDs comparing high and low pressure cases

The particulate formation mechanism under homogeneous conditions may be due to in part to unburnt hydrocarbons stored in the crevices (particularly the ring pack) being released into the combustion chamber during the expansion stroke. This unburnt fuel enters a low oxygen environment at temperatures appropriate for soot formation (1500 K to 1900 K). Higher temperatures late during the expansion stroke and the exhaust stroke will increase the nucleation rate and growth rates as the unburnt fuel is released from the crevices and mixed with the combustion products. This would help explain the higher particle numbers seen for the low intake pressure conditions, which have higher temperatures in the second half of the expansion stroke. The relatively low oxygen concentration in the combustion products, even for the lean condition, will limit the oxidation rate of particulate formed at this time.

Intake Temperature

If equivalence ratio is held constant, cases with higher intake temperature result in a higher number of small particulates and a nearly identical number of large particulates. The two runs that show the temperature trend the best are the two rich, high intake pressure cases. The thermodynamic data for these two runs is shown in Figure 10. The higher intake

temperature resulted in a temperature that was ~40 K higher than the low intake temperature case throughout the cycle. The low temperature case, however, resulted in a slightly higher pressure trace throughout the cycle, with a maximum difference of about 375 kPa between the two pressure traces. The PSDs for these two cases are shown in Figure 11. The high intake temperature case produced one to two orders of magnitude higher concentrations of particulates below 23 nm, and particle concentrations were similar (within a factor of 2 or 3) for D_m > 23 nm. Both the temperature and pressure history differ for the two cases so it is difficult to ascribe the change in concentration of the small particles to either a pressure of temperature effect. However, it is interesting to note that the inflection point near 30 nm shown in this case is seen for nearly every other case where intake temperature is changed while intake pressure and Φ are held constant. It is also useful to point out that the difference in the temperature traces for these two cases is small (~40 K), yet the effects are notable as indicated in Table 5. The increased particle numbers for the higher intake temperature agree with the previous discussion regarding intake pressure effects where it was noted that the pressure may actually be due to a difference in temperature history, and that higher temperatures during the second half of the expansion stroke may result in higher particulate numbers due to the unburnt fuel from crevices being released into the combustion chamber during this time.

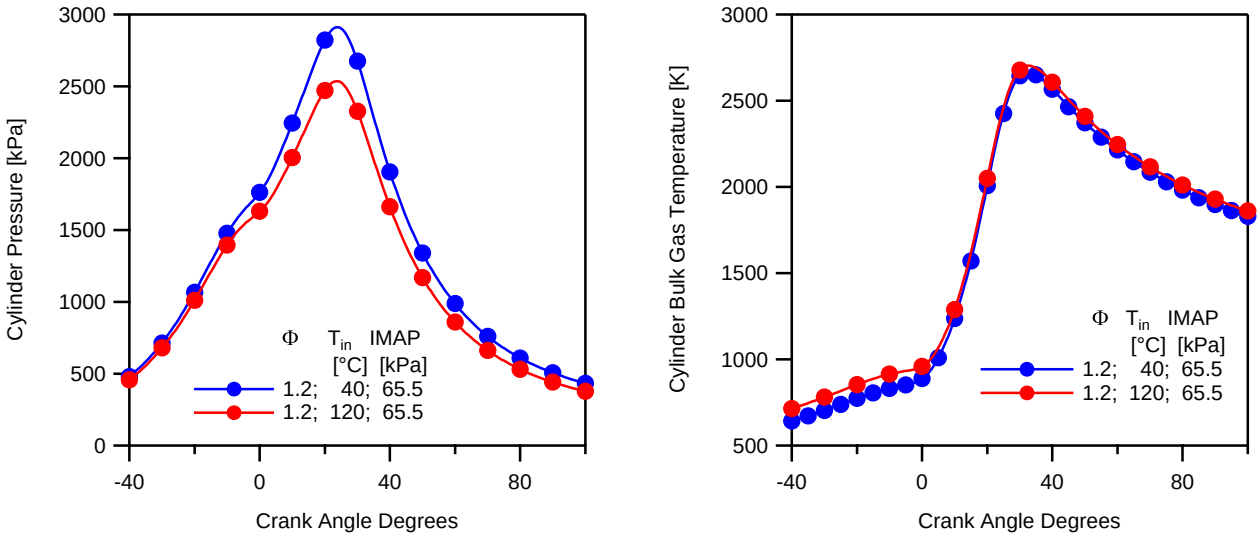

Figure 10: Temperature and pressure traces of rich, high IMAP, and varied intake temperature cases

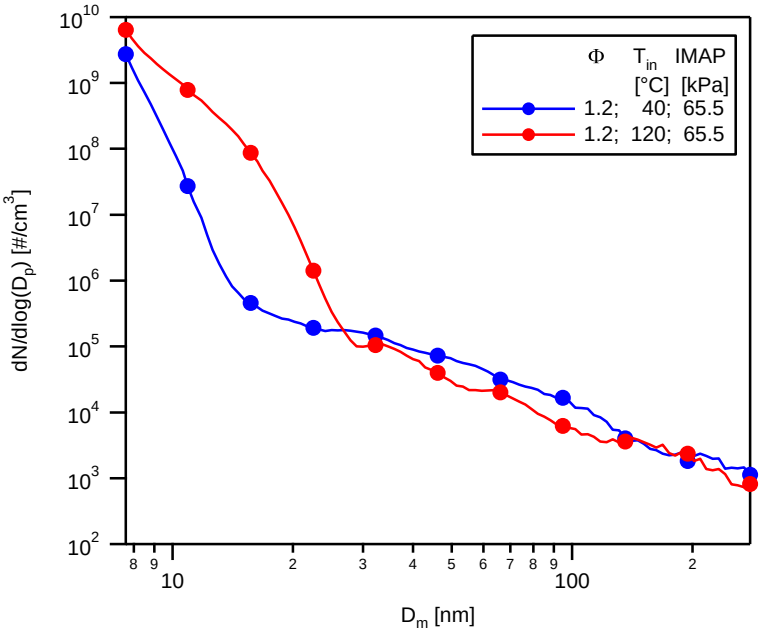

Figure 11: PSD for rich, high IMAP, and varied intake temperature cases

Total Particle Number Trends

Integrated particulate concentrations are shown in Figure 12. The integrated particulates convey much of the same information that can be gathered from the PSDs. The high pressure, low Φ cases produce by far the fewest particulates. These cases do not show the same behavior as all of the other cases as they do not exhibit an inflection point between 15 and 50 nm in the PSD corresponding to a large increase in small particles. The midpoint case produces the next fewest, probably due to a combination of all three fundamental parameters. The low pressure, low Φ cases produce slightly more particulates than the midpoint case, the high Φ, low pressure cases produce slightly more, and finally, the high pressure, high Φ cases produce the most. It can also be seen that there are only very slight differences in the integrated particulates from one temperature case to the next, with the other two variables held constant. For all of the cases, over 96% of the particles have mobility diameters $D_m < 23$ nm. This fact is less clear on the foregoing PSDs because they are plotted on a log scale. The high percentage of small particles supports the earlier point that the effect of premixing as compared to DI operation is a significant reduction in agglomeration mode particles.

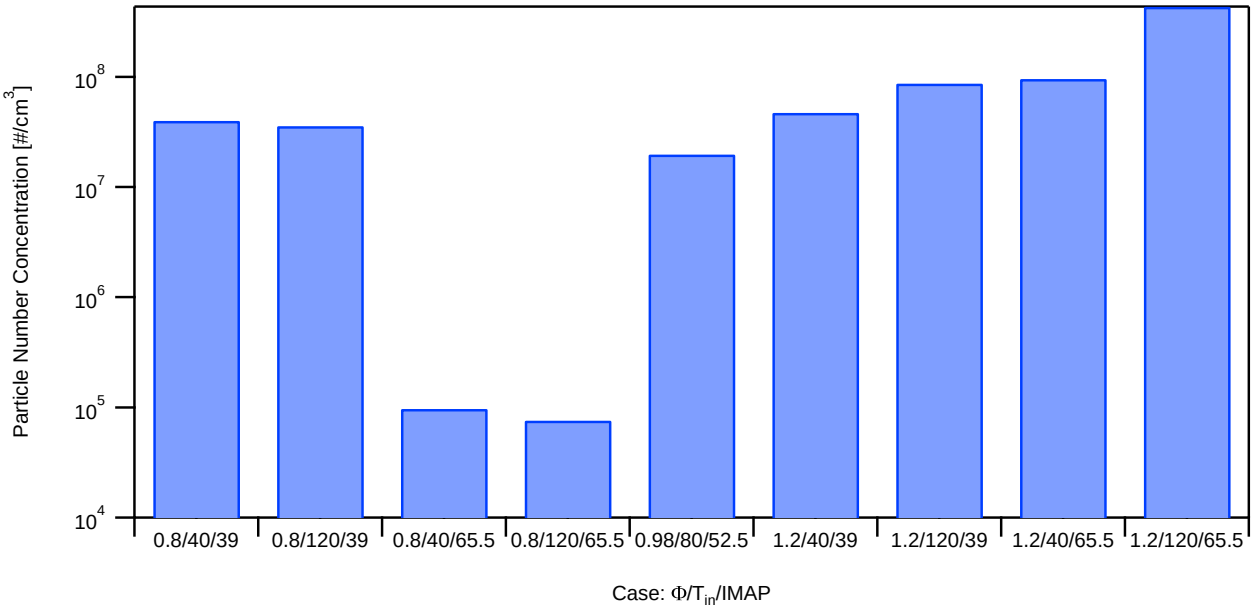

Figure 12: Integrated particulate counts

4. Conclusions

A sensitivity study was performed under completely homogeneous conditions to improve the understanding of the particulate formation processes at a fundamental level in spark-ignition IC engines. The following are the key observations and conclusions from the study.

1. All three variables tested were shown to have an effect on the PSD and total particle number. There were also strong interactions between the variables due to the fact that simple variation of one of the intake parameters actually influences both the temperature and pressure history in-cylinder.
2. Counter to observations in premixed flames a simple view of the data appeared to show decreasing particle numbers for agglomerate particles (D_m >23 nm) with increasing pressure. It is hypothesized that this effect is due to at least a fraction of the particulate not being formed during the main combustion event but actually occurring later during the expansion stroke when temperatures are in the 1500 K to 1900 K temperature range. The introduction of unburnt mixture from the crevice at this time may also be a source of particulates.
3. The results of the equivalence ratio sweep indicate that the possible onset of soot formation in the bulk gases behind the flame occurs for a C/O ratio of 0.46 or an equivalence ratio of 1.35 in agreement with high pressure laboratory flame measurements made by other researchers with other fuels.
4. The impact of increasing temperature during the expansion stroke by increasing intake air temperature appears to be an increase in the small particles with mobility diameter $D_m < 23$ nm.

In general, the transient temperature and pressure environment in the engine requires a careful consideration of the data. There may be a narrow range of crank angles where the temperature and pressure conditions are conducive to particulate

formation, so studying the variation in particulate concentrations with any single point of temperature and pressure is insufficient for understanding their roles in particle formation.

Acknowledgements
This research was funded by General Motors through the Collaborative Research Laboratory at the University of Wisconsin-Madison Engine Research Center.

References

Bonig, M., C. Felderman, et al. (1990). "Soot Formation in Premixed C2H4 Flat Flames at Elevated Pressure." The Combustion Institute **Twenty-Third Symposium (International) on Combustion**: 1581-1587.

Chan, T. W., E. Meloche, et al. (2012). "Evaluation of a Gasoline Particulate Filter to Reduce Particle Emissions from a Gasoline Direct Injection Vehicle." SAE paper 2012-01-1727: 1277-1290.

Chen, L., M. Braisher, et al. (2010). "The Influence of Ethanol Blends on Particulate Matter Emissions from Gasoline Direct Injection Engines."

Choi, K., J. Kim, et al. (2012). "Effect of the mixture preparation on the nanoparticle characteristics of gasoline direct-injection vehicles." Proceedings of the Intitution of Mechanical Engineers, Part D: Journal of Automobile Engineering: 1-11.

Farron, C., N. Matthias, et al. "Particulate Characteristics for Varying Engine Operation in a Gasoline Spark Ignited, Direct Injection Engine."

Farron, C. J. (2010). Particulate Characteristics for Varying Operation in a Fuel-Neutral, Direct Injection, Spark Ignition Engine. Master of Science, University of Wisconsin, Madison.

Frenklach, M. (2002). "Reaction mechanism of soot formation in flames." Physical Chemistry Chemical Physics **4**(11): 2028-2037.

Gatowski, J. A., E. N. Balles, et al. (1984). "Heat Release Analysis of Engine Pressure Data." SAE Technical Paper **841359**.

Haynes, B. S. and H. G. Wagner (1981). "Soot Formation." Progress in Energy and Combustion Science **7**(4): 229-273.

He, X., M. A. Ratcliff, et al. (2012). "Effects of Gasoline Direct Injection Engine Operating Parameters on particle Number Emissions." Energy & Fuels **26**: 2014-2027.

Hsieh, W. D., R. H. Chen, et al. (2002). "Engine performance and pollutant emission of an SI engine using ethanol-gasoline blended fuels." Atmospheric Environment **36**(3): 403-410.

Joo, H. I. and O. L. Gulder (2009). "Soot formation and temperature field structure in co-flow laminar methane-air diffusion flames at pressures from 10 to 60 atm." Proceedings of the Combustion Institute **32**: 769-775.

Kayes, D. and S. Hochgreb (1999). "Mechanisms of Particulate Matter Formation in Spark-Ignition Engines. 1. Effect of Engine Operating Conditions." Environmental Science & Technology **33**(22): 11.

Kayes, D. and S. Hochgreb (1999). "Mechanisms of Particulate Matter Formation in Spark-Ignition Engines. 2. Effect of Fuel, Oil, and Catalyst Parameters." Environmental Science & Technology **33**(22): 3968-3977.

Lee, J., R. Patel, et al. (2009). "Effect of Biofuels on Nanoparticle Emissions from Spark- and Compression-ignited Single-cylinder Engines with Same Exhaust Displacement Volume." Energy & Fuels **23**: 4363-4369.

Liu, F. S., K. A. Thomson, et al. (2006). "Numerical and experimental study of an axisymmetric coflow laminar methane-air diffusion flame at pressures between 5 and 40 atmospheres." Combustion and Flame **146**(3): 456-471.

Maricq, M. M., D. H. Podsiadlik, et al. (1999). "Particulate Emissions from a Direct-Injection Spark-Ignition (DISI) Engine."

Matthias, N., C. Farron, et al. (2011). "Particulate Matter Sampling and Volatile Organic Compound Removal for Characterization of Spark Ignited Direct Injection Engine Emissions." SAE Technical Paper **2011-01-2100**.

Mauss, F. and H. Bockhorn (1995). "Soot Formation in Premixed Hydrocarbon Flames: Prediction of Temperature and Pressure Dependence." Zeitschrift fr physikalische Chemie, Bd. **188**: 45-60.

Melton, T., F. Inal, et al. (2000). "The Effects of Equivalence Ratio on the Formation of Polycyclic Aromatic Hydrocarbons and soot in Premixed Ethan Flames." Combustion and Flame **121**: 671-678.

Myung, C. L. and S. Park (2012). "Exhaust Nanoparticle Emissions From Internal Combustion Engines: A Review." International Journal of Automotive Technology **13**(1): 9-22.

Piock, W., G. Hoffmann, et al. (2011). "Strategies Towards Meeting Future Particulate Matter Emission Requirements in Homogeneous Gasoline Direct Injection Engine." SAE Technical Paper **2011-01-1212**.

Price, P., B. Twiney, et al. (2007). "Particulate and Hydrocarbon Emissions from a Spray Guided Direct Injection Spark Ignition Engine with Oxygenate Fuel Blends."

Sakai, S., M. Hageman, et al. (2013). "Effect of Equivalence Ratio on the Particulate Emissions from a Spark-Ignited, Direct-Injected Gasoline." SAE Technical Paper **2013-01-1560**.

UN (2010). "Regulation No. 83, Uniform provisions concerning the approval of vehicles with regard to the emission of pollutants according to engine fuel requirements." Regulation No. 83, Uniform provisions concerning the approval of vehicles with regard to the emission of pollutants according to engine fuel requirements.

Zhao, F., M. C. Lai, et al. (1999). "Automotive spark-ignited direct-injection gasoline engines." Progress in Energy and Combustion Science **25**: 437-562.